A&A 608, A12 (2017)
DOI: 10.1051/0004-6361/201730504

Astronomy & Astrophysics

Solid CO_2 in quiescent dense molecular clouds

Comparison between *Spitzer* and laboratory spectra

T. Suhasaria[1], G. A. Baratta[2], S. Ioppolo[3], H. Zacharias[1], and M. E. Palumbo[2]

[1] Physikalisches Institut, Westfälische Wilhelms Universität, Wilhelm Klemm Straße 10, 48149 Münster, Germany
[2] INAF–Osservatorio Astrofisico di Catania, via Santa Sofia 78, 95123 Catania, Italy
e-mail: mepalumbo@oact.inaf.it
[3] School of Physical Sciences, The Open University, Walton Hall, Milton Keynes MK7 6AA, UK

Received 26 January 2017 / Accepted 27 June 2017

ABSTRACT

Context. Carbon dioxide (CO_2) is one of the most abundant species detected in icy grain mantles in star forming regions. Laboratory experiments have shown that CO_2 molecules are efficiently formed in the solid state under interstellar conditions. Specifically, solid CO_2 can be formed through energetic (e.g. UV photolysis, electron and ion bombardment) and non-energetic mechanisms (atom-addition reactions).
Aims. Here we investigate the role of low-energy cosmic-ray bombardment in the formation of solid CO_2 in quiescent dense molecular clouds.
Methods. We performed laboratory experiments to study the formation of CO_2 after ion irradiation with 200 keV H^+ of astrophysical relevant ice mixtures. Laboratory spectra are used to fit the profile of the CO_2 bending mode band observed at about 15.2 μm (660 cm^{-1}) by the *Spitzer* Space Telescope in the line of sight to background sources.
Results. From a qualitative point of view, good fits to observations are obtained by considering either three or four laboratory components. From a quantitative point of view, a better result is obtained with four components, i.e. when a spectrum of CO_2 formed after ion irradiation of CH_3OH ice is added to the fitting procedure.
Conclusions. Our results support the hypothesis that energetic processing of icy grain mantles is an efficient formation mechanism of CO_2 ice also in quiescent dark cloud regions, and indirectly suggest the presence of CH_3OH in icy grain mantles in interstellar cold regions.

Key words. astrochemistry – molecular processes – methods: laboratory: solid state – techniques: spectroscopic – ISM: molecules – ISM: lines and bands

1. Introduction

Solid carbon dioxide (CO_2) is an important constituent of icy grain mantles in the interstellar medium (ISM) with an abundance of 10–50% with respect to water ice (H_2O; Gerakines et al. 1999; Nummelin et al. 2001; Boogert et al. 2015).

Interstellar solid CO_2 has been detected in the mid-infrared through its two active fundamental vibration modes, e.g. the ν_3 stretching mode at 4.27 μm (2340 cm^{-1}) and the ν_2 bending mode at 15.2 μm (660 cm^{-1}). The bending mode feature is especially sensitive to the ice temperature and composition (polar and apolar mixtures, e.g. Ehrenfreund et al. 1996), but it has a weaker band strength than the stretching mode. The detection of the combination modes $\nu_1 + \nu_3$ and $2\nu_2 + \nu_3$ at 3707 cm^{-1} and 3600 cm^{-1} toward the protostellar object S140:IRS1 was reported by Keane et al. (2001). More than two decades ago, interstellar CO_2 was first detected in the solid phase by the low-resolution ($\lambda/\Delta\lambda$ in the range 10 to 60) Infrared Astronomical Satellite (IRAS) by the vibrational bending mode (d'Hendecourt & Jourdain de Muizon 1989). With the advent of the short-wavelength spectrometer (SWS) on board the Infrared Space Observatory (ISO) in 1995, detection of CO_2 was made easier with a better resolution ($\lambda/\Delta\lambda \sim 500$ and 1000). Soon solid CO_2 was found to be ubiquitous in a variety of different astronomical environments. In particular, it was found toward the Galactic Centre (de Graauw et al. 1996), massive protostars (Gerakines et al. 1999; Gibb et al. 2004), low-mass young stellar objects (YSOs; Nummelin et al. 2001), and toward some background stars (Whittet et al. 1998). ISO observations toward cold, quiescent dark clouds were limited, however, because of the characteristic faintness of the sources and the sensitivity of the SWS instrument (Valentijn & Thi 2000). In addition, fringing was often present in standard processed SWS data (Nummelin et al. 2001). More recently, observations of the CO_2 bending mode band obtained with the Infrared Spectrograph (IRS) aboard the *Spitzer* Space Telescope allowed the identification of CO_2 towards faint sources in dark quiescent dense molecular clouds (Werner et al. 2004).

Despite the ubiquitous presence of CO_2 in the interstellar medium, its formation route is highly debated, especially in cold, dark quiescent dense molecular clouds. The CO_2 molecule is more abundant in the solid phase than in the gas phase (van Dishoeck et al. 1996; Boonman et al. 2003), which indicates that it is formed on the surface of dust grains by grain surface reactions and/or energetic processing (Nummelin et al. 2001). Potential non-energetic formation routes in the solid phase have been discussed in many laboratory experiments, theoretical models, and observations. Whittet et al. (1998) suggested that observation of CO_2 in the quiescent dark cloud towards the line of sight of Elias 16, a field star, is solely due to

chemical reactions occurring without the input of energy. They further argued that CO_2 formation can occur without the radiation from a local embedded protostar and since the line of sight is a field star, which is behind a dense molecular cloud, they assumed that local chemical reactions around ice mantles are not triggered by energetic processing.

Theoretical models and laboratory experiments are primarily based on these two reaction schemes:

$$CO + O \rightarrow CO_2 \quad (1)$$

$$CO + OH \rightarrow CO_2 + H. \quad (2)$$

Reaction (1) has been suggested as the simplest route to CO_2 formation by Tielens & Hagen (1982). Furthermore, there is a high reaction barrier for the formation of CO_2 in the gas phase, which can be lowered on surfaces via hot O-atom or Eley-Rideal mechanism (Talbi et al. 2006; Goumans et al. 2008). Laboratory experiments also suggest that the reaction is feasible upon heating, or via reaction in water pores or under a water ice cap (Roser et al. 2001). However, Raut & Baragiola (2011) have shown by means of infrared spectroscopy and micro-gravimetry analysis that only a small quantity of CO_2 is formed upon co-deposition of CO and thin films of O and O_2 at 20 K. The reaction of O atoms to form O_3 is found to be more efficient in the above reaction. Minissale et al. (2013) have recently suggested that there is a competition between reactions (1) and (2) for efficient CO_2 formation in space. The efficiency of CO_2 formation via reaction (1) depends on the temperature of the grain surface and the abundance of O atom in the observed region. On the other hand, theoretical models and laboratory experiments both suggest that reaction (2) can be a reaction pathway to the formation of CO_2 without energetic processing. In their theoretical model, Goumans et al. (2008) suggested CO_2 formation via an HO-CO intermediate. Independent experimental studies (Oba et al. 2010; Ioppolo et al. 2011; Noble et al. 2011) further strengthen this reaction pathway. More recently, the laboratory work of Ioppolo et al. (2013a) has shown that reaction (2) is ten times more efficient than reaction (1) under the same interstellar relevant conditions. Minissale et al. (2015) have suggested an efficient CO_2 formation via the following reaction scheme in the solid phase:

$$H_2CO + O \rightarrow CO_2 + H_2. \quad (3)$$

The role of energetic processing such as irradiation by UV photons, ions, and electrons in the formation of CO_2 in the solid phase has been extensively studied in several laboratory experiments (d'Hendecourt et al. 1986; Moore et al. 1991; Bernstein et al. 1995; Gerakines et al. 1996; Ehrenfreund et al. 1997; Palumbo et al. 1998; Watanabe & Kouchi 2002; Mennella et al. 2004; Mennella et al. 2006; Loeffler et al. 2005; Jamieson et al. 2006; Ioppolo et al. 2009; Ioppolo et al. 2013b; Laffon et al. 2010; Garozzo et al. 2011). Quiescent dark molecular clouds are shielded from the external UV field. However, cosmic rays can penetrate dense clouds and therefore induce energetic processing in these regions. Moreover, cosmic rays can induce an internal UV field through the interaction with molecular hydrogen gas in dense clouds (Prasad & Tarafdar 1983; Jenniskens et al. 1993; Mennella et al. 2003; Shen et al. 2004).

In this manuscript first we present the experimental results relative to CO_2 formation in three different ice mixtures by ion irradiation with 200 keV H^+ at low temperature. Then we use laboratory spectra to fit the profile of the CO_2 bending mode band observed by the *Spitzer* Space Telescope in the line of sight to quiescent dark cloud regions to understand the chemical processes in the earliest stages of star formation. In the fitting procedure, in addition to the new experiments here presented, we used some selected laboratory spectra, which are available in the Catania database[1]. Furthermore, we discuss the quality of the fits obtained and the quantitative contribution of each ice component to the fit including solid CH_3OH in the formation of CO_2 upon energetic processing of the ice.

2. Experimental methods

The experimental results presented here were obtained in the Laboratorio di Astrofisica Sperimentale at INAF – Osservatorio Astrofisico di Catania (Italy). The experiments were performed in a stainless steel ultra-high vacuum (UHV) chamber with a base pressure better than 10^{-9} mbar. A closed-cycle helium cryostat is attached to the UHV chamber and is used to cool a KBr substrate which is in thermal contact with the sample holder of the cryostat. The substrate temperature can be varied between 16 and 300 K. The chamber is also connected to a 200 kV ion implanter (Danfysik 1080) which can produce ions in the energy range between 30 and 200 keV (or 400 keV for double ionization). The ion implanter is optimized to accelerate ions from gas phase species (such as H, He, Ar, C, O, and N). In the present study all samples were irradiated with 200 keV H^+.

Pure gases or mixtures are admitted into the main chamber by means of a needle valve and deposited onto the KBr substrate at low temperature. A He-Ne laser (λ = 543.5 nm) is used to monitor the ice thickness on the substrate during accretion. More details on this procedure can be found in Baratta & Palumbo (1998) and Urso et al. (2016). Furthermore, ices are studied by using a Fourier transform infrared (FTIR) spectrometer (Bruker Vertex 70) which works in the spectral range between 7500 and 400 cm^{-1} (1.33–25 μm) with a resolution of 1 cm^{-1}. The substrate forms an angle of 45° with respect to both the ion beam and the IR beam. This allows the acquisition of transmittance spectra without needing to turn the sample. Spectra are taken before and after irradiating the sample at low temperature (17 K) and also at selected higher temperatures after annealing the substrate up to 90 K. A schematic depiction of the UHV chamber is presented in Fig. 1.

The experiments performed in this work are listed in Table 1. Spectra obtained in transmittance units (I_f) are converted into optical depth units as $\tau(\nu) = \ln(I_0/I_f)$, where I_0 is the normalization continuum. Furthermore, the column density (N, molecules cm^{-2}) of each species is calculated from the respective band area $\int \tau(\nu)d\nu$ of each IR band divided by the band strength (A) value obtained from literature. All band strength values used in the current work are listed in Table 2.

The ion beam is electrostatically swept and produces a spot on the sample which is larger than the area probed by the IR beam. The penetration depth of the impinging ions (200 keV H^+) is greater than the sample thickness (about 1 μm) as verified using the SRIM code (Ziegler et al. 2008). Macroscopic heating of the substrate is avoided by keeping the ion beam current density lower than 1 $\mu A\ cm^{-2}$.

A rotatable polarizer is placed in the path of the IR beam, which enables us to subsequently record spectra in P (i.e. the electric vector is parallel to the plane of incidence) and S (i.e. the electric vector is perpendicular to the plane of incidence) mode where the plane of incidence is the plane of the paper in Fig. 1.

[1] http://www.oact.inaf.it/weboac/labsp/

Table 1. New experiments performed in this work.

Mixture	Thickness (μm)	Ion and energy	Stopping power[a] (eV cm^2/16u)	Max dose (eV/16u)
H_2O:CO = 8:1	0.8	H^+, 200 keV	2.72×10^{-14}	50
CO:CH_4:N_2 = 1:1:1	1.0	H^+, 200 keV	2.60×10^{-14}	105
H_2O:CH_4:NH_3 = 1:1:1	1.0	H^+, 200 keV	3.76×10^{-14}	600

Notes. [(a)] The average stopping power through the sample was obtained using SRIM software (Ziegler et al. 2008).

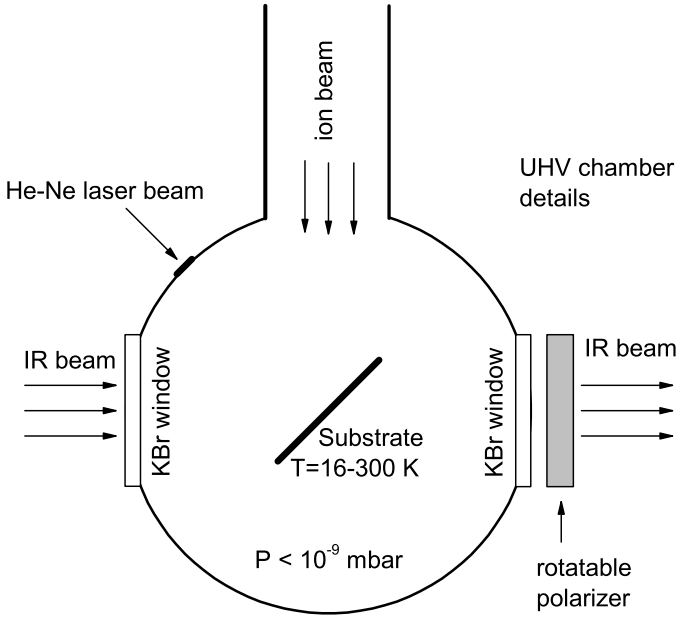

Fig. 1. Schematic depiction of the UHV chamber.

Background spectra of the bare cold substrate are recorded before ice deposition in both P and S modes and are subsequently subtracted from each of the following P and S spectra of the ice.

The energy released to the sample by the impinging ions (dose) is given in eV/16u, where u is the unified atomic mass unit defined as 1/12 of the mass of an isolated atom of carbon-12. This dose is obtained by calculating the average stopping power (eV cm^2/molecule) using the SRIM software and multiplying it by the ion fluence (ions cm^{-2}) measured during each experiment. As discussed by Strazzulla & Johnson (1991), the dose given in units of eV per small molecule (16u) is a convenient way to characterize chemical changes and to compare the results obtained by irradiating different samples.

As discussed in previous studies (Ioppolo et al. 2009, 2013b), the profile of the CO_2 bending mode band produced after ion bombardment does not depend on the polarization mode. When the band profile does not depend on the polarization mode, laboratory transmittance spectra directly correlate with the variation of the absorption coefficient in the solid sample (Baratta et al. 2000; Palumbo et al. 2006). Hence, a direct comparison between laboratory spectra and astronomical observations is possible. In this work, only spectra in P mode are taken into account owing to their better signal-to-noise ratio.

In addition to the new experiments presented here, we used some selected laboratory spectra which are available in the Catania database to fit the astronomical observations (Ioppolo et al. 2009, 2013b). A full list of the laboratory spectra considered in this work is given in Table 3. As an example, the spectra relative

Table 2. List of the band strength (A) values used.

Molecule	Band (cm^{-1})	A (cm molecule^{-1})	Reference
H_2O	3300	20×10^{-17}	1
CH_4	3010	9.5×10^{-18}	2
CO_2	2345	7.6×10^{-17}	3
CO	2139	1.1×10^{-17}	4
CH_4	1310	6.4×10^{-18}	2
NH_3	1070	1.7×10^{-17}	5
CH_3OH	1020	1.3×10^{-17}	6
H_2O	800	2.8×10^{-17}	7
CO_2	660	1.1×10^{-17}	8

References. (1) Allamandola et al. (1988); (2) Mulas et al. (1998); (3) Yamada & Person (1964); (4) Jiang et al. (1975); (5) Lacy et al. (1998); (6) Palumbo et al. (1999); (7) Hudgins et al. (1993); (8) Gerakines et al. (1995).

Table 3. Laboratory spectra used to fit observations.

Sample	Reference
H_2O:CO = 8:1 +200 keV H^+, T = 17 K	1
CO:CH_4:N_2 = 1:1:1 +200 keV H^+, T = 17 K	1
H_2O:CH_4:NH_3 = 1:1:1 +200 keV H^+, T = 17 K	1
H_2O on carbon grains +200 keV H^+, T = 17 K	2
CO +200 keV H^+, T = 16 K	3
CO +200 keV H^+, T = 40 K	3
CO:H_2O = 10:1 +200 keV H^+, T = 16 K	3
CO:H_2O = 10:1 +200 keV H^+, T = 40 K	3
CO:N_2 = 8:1 +200 keV H^+, T = 16 K	3
CO:N_2 = 8:1 +200 keV H^+, T = 40 K	3
CO:N_2 = 1:1 +200 keV H^+, T = 16 K	3
CO:N_2 = 1:1 +200 keV H^+, T = 40 K	3
CH_3OH +200 keV H^+, T = 16 K	4
CH_3OH +200 keV H^+, T = 40 K	4

References. (1) This work; (2) Ioppolo et al. (2013b); (3) Ioppolo et al. (2009); (4) Modica & Palumbo (2010).

to pure CO after bombardment with 200 keV H^+ at 16 K, a mixture CO:N_2 = 1:1 after bombardment with 200 keV H^+ at 16 K, and pure CH_3OH after bombardment with 200 keV H^+ at 16 K are shown in Fig. 2. The main features formed after bombardment are labelled. The vertical grey arrows indicate the spectral range where most of the features assigned to carbon chain oxides and nitrogen oxides, also formed after bombardment, occur. A detailed description of the spectra listed in Table 3 is given by Palumbo et al. (2008), Modica & Palumbo (2010), Sicilia et al. (2012), Ioppolo et al. (2013b), and Kaňuchová et al. (2016).

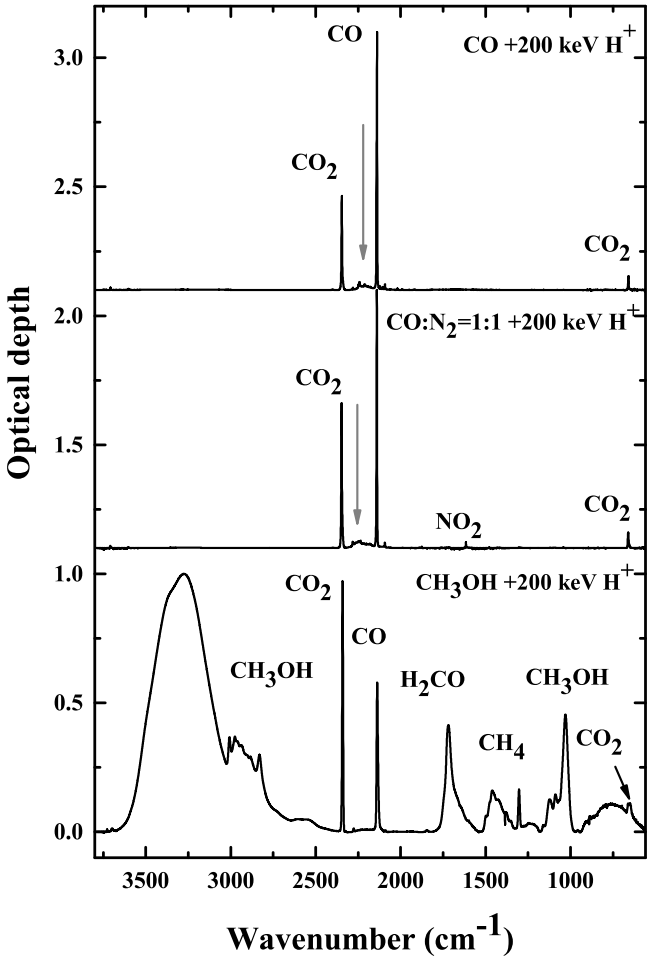

Fig. 2. Selected infrared spectra, in the range 3800–560 cm^{-1}, used in the fitting procedure. *From top to bottom* the spectra refer to pure CO after bombardment with 200 keV H^+ at 16 K, a mixture CO:N_2 = 1:1 after bombardment with 200 keV H^+ at 16 K, and pure CH_3OH after bombardment with 200 keV H^+ at 16 K. Spectra are normalized to their maximum optical depth value and are shifted for clarity. The main features formed after bombardment are labelled. The vertical grey arrows indicate the spectral range where most of the features assigned to carbon chain oxides and nitrogen oxides occur. A detailed description of these spectra is given by Palumbo et al. (2008), Sicilia et al. (2012), and Modica & Palumbo (2010).

3. Results

3.1. Experimental results

3.1.1. H_2O:CO mixture

A H_2O:CO = 8:1 mixture is deposited onto a cold KBr substrate at 17 K and then irradiated with 200 keV H^+ to study the formation of CO_2. Figure 3 shows the column density of CO_2 divided by the initial column density of CO, $N(CO_2)/N(CO)_i$, as a function of irradiation dose. The column density of CO is calculated using the band area of the C≡O stretching mode at 2139 cm^{-1}. The column density of CO_2 is calculated using the band area of the C=O stretching mode at 2345 cm^{-1}. The corresponding band strength values (A) are listed in Table 2. As shown in Fig. 3, the CO_2 column density rapidly increases at low doses and then almost reaches an equilibrium value at the highest investigated dose. The value of the stopping power used to calculate the dose is given in Table 1.

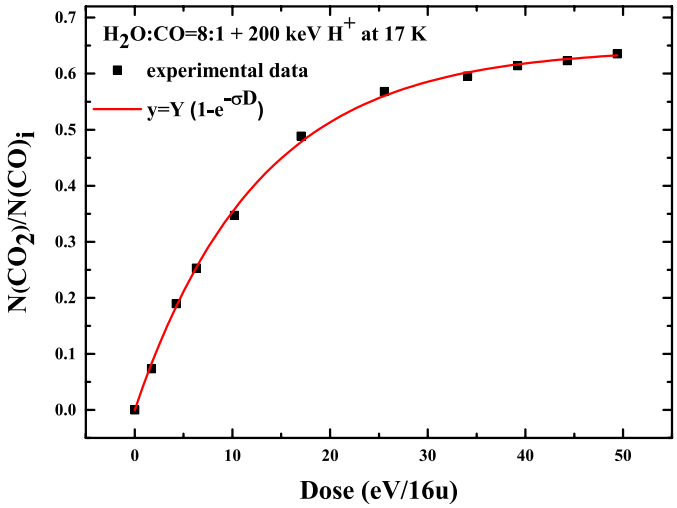

Fig. 3. Column density of CO_2 divided by the initial column density of CO after ion bombardment with 200 keV H^+ of a H_2O:CO = 8:1 mixture at 17 K. Experimental data are fitted by an exponential curve.

The experimental data relative to the formation of CO_2 are fitted by the exponential curve

$$y = Y(1 - e^{-\sigma D}), \quad (4)$$

where y is the $N(CO_2)/N(CO)_i$ ratio, Y is the asymptotic value, σ is a parameter (in 16u/eV), and D is the dose (in eV/16u). The parameter σ is often referred to as the cross-section (see Rothard et al. 2017, for a recent review) and according to chemical kinetics it can be regarded as a rate constant in units of $dose^{-1}$ instead of $time^{-1}$. The fitting procedure gives $Y = 0.64 \pm 0.01$ and $\sigma = 0.08 \pm 0.01$ 16u/eV. The value of Y obtained in this experiment is comparable to the value obtained previously by Ioppolo et al. (2009) for the same mixture irradiated with 30 keV He^+, which suggests that the equilibrium value of CO_2 produced does not depend on the energy and mass of the ion used within experimental uncertainties.

3.1.2. CO:CH_4:N_2 mixture

A mixture CO:CH_4:N_2 = 1:1:1 deposited at 17 K and irradiated by 200 keV H^+ is used to retrieve information on the formation of CO_2 in an apolar environment. Figure 4 shows the column density of CO_2 divided by the initial column density of CO, $N(CO_2)/N(CO)_i$, as a function of irradiation dose. The column densities of CO and CO_2 are calculated following the same procedure described above (Sect. 3.1.1). The experimental data are fitted by Eq. (4) in this case as well. The fitting procedure gives $Y = 0.080 \pm 0.001$ and $\sigma = 0.027 \pm 0.001$ 16u/eV. The value of Y obtained in this experiment is similarly comparable to the value obtained previously by Ioppolo et al. (2009) for the same mixture irradiated with 30 keV He^+. This again suggests that the equilibrium value of CO_2 does not depend on the ion used.

3.1.3. H_2O:CH_4:NH_3 mixture

In order to investigate the formation of CO_2 in an ice mixture that does not contain CO, we considered a mixture of H_2O:CH_4:NH_3 = 1:1:1 at 17 K. Figure 5 shows the column density of CO_2 after ion bombardment of 200 keV H^+ divided by the initial column density of CH_4. The column densities of CH_4 and CO_2 are calculated using the band area of the C-H stretching

Table 4. Observed column densities (in units of 10^{17} cm^{-2}) of CO, H_2O, CO_2, and CH_3OH and A_V values for the lines of sight studied here.

Source ID/2MASS ID	Other ID	Cloud	A_V (mag)	$N(CO)^a$	$N(H_2O)^b$	$N(CO_2)^c$	$N(CH_3OH)^d$
041443.5+281708		Taurus	16.2 ± 1.5			2.7	
042630.7+243637		Taurus	17.8 ± 1.5	7.4	16.4	3.0	
042930.2+265827		Taurus	11.4 ± 1.5			1.9	
043213.2+242910		Taurus	20.9 ± 1.5	7.5	22.5	3.6	
043728.2+261024	Tamura 2	Taurus	6.3 ± 1.5		4.0	1.0	
043926.9+255259	Elias 15	Taurus	15.3 ± 0.5	4.1	15.0	2.5	
J04393886+2611266	Elias 16	Taurus	24.1 ± 0.5	6.5	25.7^e	5.4	<0.25
J18300061+0115201	CK2, EC 118	Serpens	34 ± 4	16.2	35	9.9	<2.1
J21472204+4734410	Q21-1	IC 5146	27 ± 1	7.1	25.2	8.7	0.24

Notes. [(a)] From published observations (Chiar et al. 1994, 1995; Pontoppidan et al. 2003; Knez et al. 2005) as reported by Whittet et al. (2007, 2009). [(b)] From published observations (Eiroa & Hodapp 1989; Murakawa et al. 2000; Smith et al. 1993; Whittet et al. 1988) as reported by Whittet et al. (2007, 2009). [(c)] From published observations as reported by Whittet et al. (2007, 2009). [(d)] From published observations (Chiar et al. 2011; Boogert et al. 2011). [(e)] Average value from 3 μm spectra of Whittet et al. (1988), Smith et al. (1993), and Murakawa et al. (2000) as reported by Whittet et al. (2009).

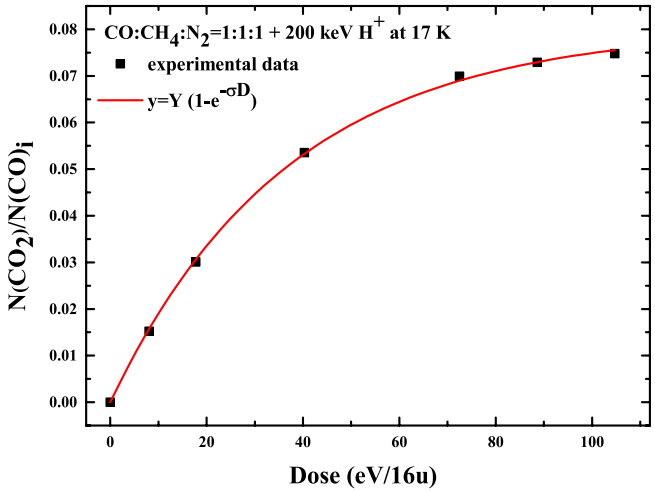

Fig. 4. Column density of CO_2 divided by the initial column density of CO after ion bombardment of a CO:CH_4:N_2 = 1:1:1 mixture at 17 K. Experimental data are fitted by an exponential curve.

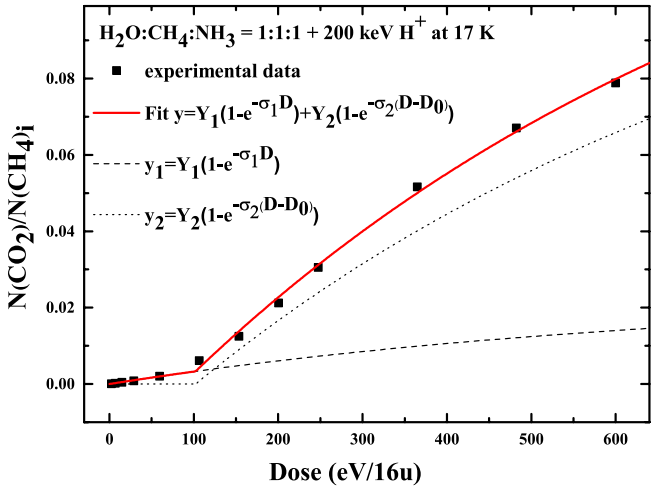

Fig. 5. Column density of CO_2 divided by the initial column density of CH_4 after ion bombardment of a H_2O:CH_4:NH_3 = 1:1:1 mixture at 17 K. Experimental data are fitted by two exponential curves.

mode of CH_4 at 3010 cm^{-1} and the C=O stretching mode of CO_2 at 2345 cm^{-1} together with the band strength values (A) listed in Table 2. We see that there is a clear difference in the formation trend of CO_2 at low doses with respect to higher doses. The experimental data are therefore fitted by two exponential curves with a threshold dose (D_0) to take into account the change in the CO_2 production rate. The variation of CO_2 formation rate at different doses has been observed previously by Ioppolo et al. (2009) in a H_2O:CH_4 = 4:1 mixture irradiated with 30 keV He^+, which suggests that regardless of the type of ion used during irradiation, this trend generally occurs for CH_4-containing ice mixtures. More hydrocarbons are formed at low doses, as shown by Baratta et al. (2002) for pure CH_4 ice, while column densities of CO and CO_2 are low. At higher doses, the production rate of CO and CO_2 increases, while the yield of hydrocarbons decreases. In particular, we found for $D \leq D_0$

$$y = Y_1(1 - e^{-\sigma_1 D}), \quad (5)$$

and for $D > D_0$

$$y = Y_1(1 - e^{-\sigma_1 D}) + Y_2(1 - e^{-\sigma_2 (D - D_0)}), \quad (6)$$

where D_0 is the threshold dose. The fitting procedure gives D_0 = 102 ± 12 eV/16u, Y_1 = 0.02 ± 0.02, σ_1 = 0.001 ± 0.001 16u/eV, Y_2 = 0.14 ± 0.04, and σ_2 = 0.0013 ± 0.0004 16u/eV.

3.2. Fit to observations

Previous studies compared the profile of the CO_2 bending mode observed towards high-mass (Ioppolo et al. 2009) and low-mass (Ioppolo et al. 2013b) YSOs and one field star (CK2) with the laboratory spectra of CO_2 formed after ion bombardment of C- and O-bearing ice samples. It was also extensively discussed that the CO_2 bending mode band profile is strongly sensitive to ice mixture and temperature. Here, we extend on the work of Ioppolo et al. (2009, 2013b) by selecting several sources along quiescent dense molecular clouds (i.e. background sources) and using the CO_2 vibrational bending mode band as observed by the IRS of the *Spitzer* Space Telescope (Bergin et al. 2005; Knez et al. 2005; Whittet et al. 2007, 2009) to characterize the formation of CO_2 after energetic processing of interstellar relevant ices.

The selected lines of sight are listed in Table 4. As discussed by Whittet et al. (2007, 2009), the profiles of the CO_2 bending

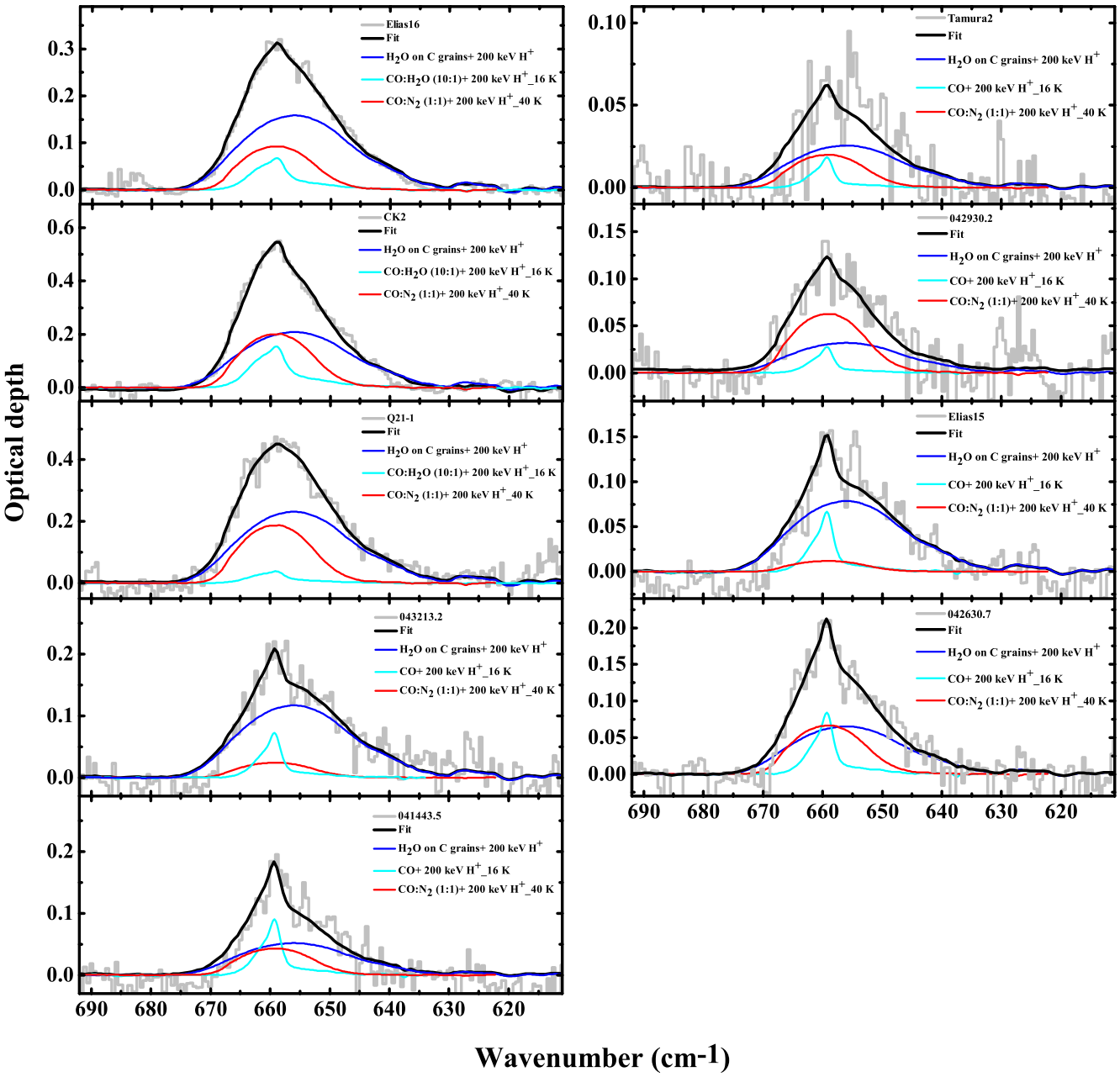

Fig. 6. Three-component fit. Laboratory spectra are: H_2O on C-grains +200 keV H^+, CO (pure or mixed) +200 keV H^+ (16 K), and CO (pure or mixed) +200 keV H^+ (40 K).

mode band towards these lines of sight are very similar to each other and there is no clear evidence for structures that could be indicative of thermal processing of ices. We followed a systematic fitting procedure of the observational spectra with laboratory spectra using the software Polyfit, which we developed in-house, which uses a linear combination of up to five different laboratory spectra to obtain the best fit. In all the figures which show the results of the fitting procedure, observational data are always represented by a step horizontal centre light grey line, the black solid line is the best fit result, and different laboratory components are represented by solid thick coloured lines. It is important to stress that the computed fits are not unique, and only represent a possible solution that can reproduce the observed CO_2 vibrational bending mode profile towards quiescent dark clouds. As shown in Fig. 6, a reasonable agreement is reached between the laboratory spectra and the observed spectra by using three fit components of the CO_2 bending mode band profile obtained after irradiation of relevant ice mixtures.

Our choice of fit components is based on observational evidence. In dense molecular clouds, H_2O, CO, and other molecules appear as a frozen mantle on the surface of dust grains, as shown by the 3.1 μm and 4.67 μm absorption features of solid H_2O and CO ices (Whittet et al. 1988; Chiar et al. 1995), respectively. Cosmic rays can penetrate quiescent dark molecular clouds that induce processing of the ices and produce CO_2; this molecule has a comparable formation threshold to that of H_2O (Bergin et al. 2005; Boogert et al. 2015), which suggests that there is a close chemical connection between these two species. Moreover, in the initial stages of cold quiescent dark clouds, H_2O is formed on the grain surface (van Dishoeck et al. 2013) and previous laboratory experiments have shown efficient CO_2 production by ion irradiation of H_2O on C-grain surfaces

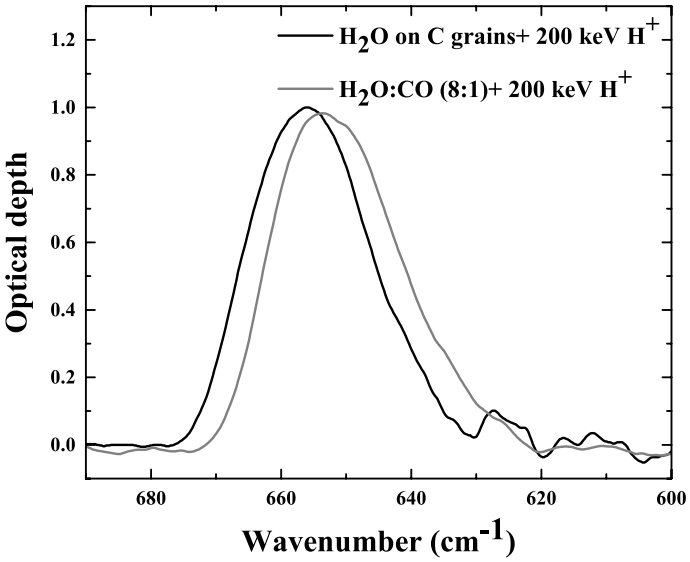

Fig. 7. Comparison between the band profile of the CO_2 bending mode in H_2O on C-grains +200 keV H^+ and in a H_2O:CO (8:1) mixture +200 keV H^+.

(Mennella et al. 2004; Raut et al. 2012; Ioppolo et al. 2013b). Taking into consideration all these factors, we used CO_2 formed after irradiation of H_2O on C-grains as a common component that is used to fit a broad contribution to the band profile, as discussed by Ioppolo et al. (2013b). Moreover, some CO may be trapped in a water-rich ice before its "catastrophic" freeze-out at higher A_V. Therefore, we also included new experimental results of CO_2 formation by proton irradiation of a H_2O:CO = 8:1 mixture. Figure 7 shows that the CO_2 vibrational bending mode profile obtained by irradiating a H_2O:CO = 8:1 mixture is very similar to ion irradiation spectra of H_2O on C-grains. Both profiles are broad and either of them can be used as the polar component. The other two components are a combination of either pure CO ice or CO mixed with H_2O or N_2 ice in different proportions irradiated with 200 keV H^+. In all these fits we have always considered the spectra of CO_2 formed after irradiation of either pure CO or CO containing mixtures at 16 K (cold component), which fits the narrow feature of the observed band profile at 660 cm^{-1} and the spectra of the same irradiated ice samples warmed up to 40 K (warm component), which fits the weak shoulder of the observed profile at about 655 cm^{-1}. The laboratory spectra used for the systematic fit of the observed spectra are listed in Table 3.

CH_3OH ices. Solid methanol (CH_3OH) has been detected in the line of sight to YSOs and background sources (e.g. Boogert et al. 2015). Its abundance with respect to solid H_2O ranges between <1% and 31% towards YSOs and between <1% and 12% towards background sources, with a median value of 6–9%, which seems to be independent of the nature of the source. It is generally accepted that CH_3OH forms on grain surfaces after CO hydrogenation (Watanabe et al. 2004; Fuchs et al. 2009). With this in mind, we also present four-component fits computed by adding the CO_2 bending mode profile obtained after irradiation of pure CH_3OH ice at 16 K as an additional component to the three-component fits reported in Fig. 6. The four-component fits, shown in Fig. 8, have been computed only for the three observational spectra which have the best signal-to-noise ratio and have an observed CH_3OH column density given in Table 4.

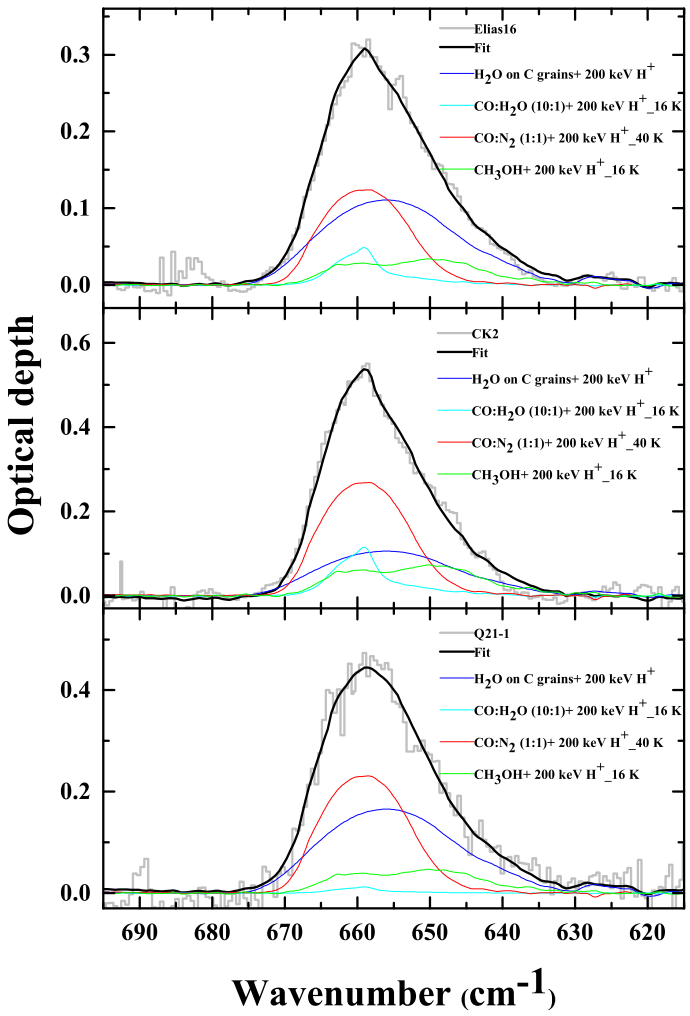

Fig. 8. Four-component fit. Laboratory spectra are: H_2O on C-grains +200 keV H^+, CO mixtures +200 keV H^+ (16 K), and CO mixtures +200 keV H^+ (40 K) and CH_3OH +200 keV H^+ (16 K).

3.3. Observational constraints

In Table 4, we have listed all the sources along with the observed column densities of H_2O, CO, CO_2, CH_3OH, and the visual extinction A_V for each selected line of sight. In order to check that our fitting analysis provides us with the best fit and also a physically meaningful comparison between observational and laboratory spectra, we calculated the expected column density of CO_2 after cosmic ion bombardment of H_2O on C-grains, pure and mixed CO, and CH_3OH using Eqs. (7), (8a), and (9), respectively,

$$N_{\rm exp}(CO_2) = 9.3 \times 10^{15}\, A_V \quad (7)$$

$$N_{\rm exp}(CO_2) = 0.07\, N_{\rm tot}(CO) \quad (8a)$$

$$N_{\rm tot}(CO) = 9 \times 10^{-5}\, N(H_2) \quad (8b)$$

$$N(H_2) = 1.87 \times 10^{21}\, A_V \quad (8c)$$

$$N_{\rm exp}(CO_2) = 2.36\, N_{\rm obs}(CH_3OH), \quad (9)$$

where $N_{\rm obs}$ is the observed column density.

These equations are based on the results reported by Mennella et al. (2006) and Ioppolo et al. (2009, 2013b) assuming that the interstellar cloud lifetime is 3×10^7 yr. To derive the $N_{\rm tot}$(CO), we correlate it with the column density of H_2 using Eq. (8b) as suggested by Liu et al. (2013). The column density

Table 5. Expected column density (in units of 10^{17} cm^{-2}) of CO_2 obtained after irradiation of three components – H_2O on C-grains +200 keV H^+, CO (pure or mixed) +200 keV H^+ (16 K), and CO (pure or mixed) +200 keV H^+ (40 K) – and column density of CO_2 obtained from the fit for some selected sources.

Source ID/2MASS ID	Other ID	H_2O on C-grains		Apolar component	
		Expected	Fit	Expected	Fit
041443.5+281708		1.51	1.05	1.91	0.91
042630.7+243637		1.66	1.32	2.10	1.18
042930.2+265827		1.06	0.65	1.34	0.90
043213.2+242910		1.94	2.36	2.46	0.60
043728.2+261024	Tamura 2	0.59	0.52	0.74	0.33
043926.9+255259	Elias 15	1.42	1.59	1.80	0.42
J04393886+2611266	Elias 16	2.24	3.20	2.27	1.69
J18300061+0115201	CK2, EC 118	3.16	4.22	4.01	3.72
J21472204+4734410	Q21-1	2.51	4.68	3.18	2.65

Table 6. Expected column density (in units of 10^{17} cm^{-2}) of CO_2 obtained after irradiation of four components – H_2O on C-grains +200 keV H^+, CO mixtures +200 keV H^+ (16 K), CO mixtures +200 keV H^+ (40 K), and CH_3OH +200 keV H^+ at 16 K – and column density of CO_2 obtained from the fit for some selected sources.

Source ID/2MASS ID	Other ID	H_2O on C-grains +200 keV H^+		Apolar component		CH_3OH +200 keV H^+	
		Expected	Fit	Expected	Fit	Expected	Fit
J04393886+2611266	Elias 16	2.24	2.24	2.27	1.94	<0.59	0.58
J18300061+0115201	CK2, EC 118	3.16	2.14	4.01	4.26	<4.96	1.24
J21472204+4734410	Q21-1	2.51	3.18	3.18	3.00	0.57	0.80

of H_2 has been computed using Eq. (8c) following Knez et al. (2005). The CO_2 column density obtained after the fitting procedure and the expected CO_2 column density ($N_{exp}(CO_2)$) are listed in Tables 5 and 6. As discussed by Ioppolo et al. (2009, 2013b), the calculated expected column density values have to be regarded as upper limits.

4. Discussion

The bulk of interstellar ices comprises H_2O, CO, CH_3OH and CO_2. Other species, such as CH_4 and NH_3, have been detected in the line of sight to young stellar objects and although less abundant they still represent a significant fraction of the ice (between 1% and 10% with respect to H_2O; Boogert et al. 2015). With this in mind, we present the proton irradiation of the CO:CH_4:N_2 = 1:1:1 mixture and H_2O:CH_4:NH_3 = 1:1:1 to investigate CO_2 formation in such ice mixtures. Although it can be argued that the ice mixtures in these ratios are not relevant in dense molecular clouds, nonetheless such experiments can provide the values of the formation cross-section of CO_2 in proton-irradiation experiments in these mixed ices (e.g. Rothard et al. 2017), and on the other hand reveal the variation in the CO_2 bending mode band profile, due to the presence or absence of these species.

In this work we used the new experiments presented here and those from the Catania database to systematically fit the observed CO_2 band profile using the vibrational bending mode band at 15.2 μm (660 cm^{-1}). Similar fits have been computed by Ioppolo et al. (2009, 2013b) for YSOs and by Mennella et al. (2006) and Ioppolo et al. (2013b) for some field stars. Here we have extended this study to nine field sources.

Previous studies (Knez et al. 2005; Bergin et al. 2005; Whittet et al. 2009) have already compared the profile of the CO_2 bending mode band observed towards background sources with laboratory spectra of co-deposited species. In these investigations laboratory spectra of polar (e.g. H_2O:CO_2) and apolar (e.g. CO:CO_2) mixtures are considered. From a qualitative point of view the fit obtained in the present work are equivalent to those obtained in previous studies.

The comparison between laboratory spectra shows that the profile of CO_2 bands formed after ion irradiation of either CO or CH_3OH is similar to the profile of CO_2 bands when CO_2 is co-deposited with CO or CH_3OH. Similarly, the profile of the CO_2 bands formed after ion irradiation of H_2O on C-grains or H_2O:CO mixtures is similar to the profile of CO_2 bands when CO_2 is co-deposited with H_2O. However, the advantage of fitting the astronomical observations with the spectra of ion irradiated mixtures over the co-deposited mixtures is that the fit not only provides information on the chemical and physical environment in which CO_2 is present, but also gives clues to the formation process of CO_2 in ice grain mantles and allows a quantitative estimation of the reliability of the results. To the best of our knowledge, the formation of interstellar CO_2 after cosmic-ion irradiation is the only process that has been checked to give a good agreement, from a qualitative and a quantitative point of view, with observations of solid CO_2 towards high-mass (Ioppolo et al. 2009) and low-mass (Ioppolo et al. 2013b) YSOs and background sources (this work). Furthermore it can justify the presence of CO_2 concurrently in polar and apolar environments along the same line of sight.

Here we present two sets of reasonable fits, one with three components (Fig. 6) and another with four components (Fig. 8). Close examination of the CO_2 bending mode band profiles for the observed sources show that they look identical and have a single asymmetric peak (at 660 cm^{-1}) with a broad shoulder on the lower wavenumber side of the band at about 650 cm^{-1}. Since our sources are cold, dark quiescent clouds and our observed CO_2 band profile lacks a double peak, we tried our fits with cold and slightly warm components. Two-component fits obtained by irradiated H_2O-dominated (polar) and CO-dominated (apolar) component at 16 K are not sufficient to produce reasonable fits for all the sources, as suggested above. So we tried the irradiated warm CO-dominated (apolar) component at 40 K,

which reproduces the weak shoulder (at about 655 cm^{-1}) quite nicely. Reliable results with a 30 K warm component were previously obtained for the background sources CK2 and Elias 16 by Knez et al. (2005) to fit the observed CO_2 bending mode feature, and also by Chiar et al. (1994) to fit the CO stretching mode feature of the field star CK2. Hence, the choice of a slightly warm component to obtain a good fit is not unreasonable. Furthermore, if we imagine the long line of sight towards the field star then we might find a small temperature gradient along the observed line since the edges are not shielded and are more open to thermal processing. A small contribution from a warm apolar component improves the fit. In addition, we also tried to replace this component with a spectrum of irradiated CH_3OH (polar) because the shoulder can be caused by the interaction between solid CO_2 and alcohols as discussed in earlier works (e.g. Dartois et al. 1999; Gerakines et al. 1999; Pontoppidan et al. 2008). However, after taking into account the entire experimental database, we obtained better fits when we used a small contribution from both a warm apolar and a polar CH_3OH component as shown in Fig. 8. We chose the sources with the best signal-to-noise ratio to compare the three- and four-component fits.

A reasonable fit cannot be the only criterion for our assumption, so we tried to estimate quantitatively the column density of CO_2 from the fits as discussed in Sect. 3.3. The column densities of CO_2 obtained by the different components are separately calculated and are compared with the expected CO_2 column density in Tables 5 and 6 for three- and four-component fits, respectively. The fits in Figs. 6 and 8 are almost identical from the qualitative point of view, but from Tables 5 and 6, we can conclude that the fits with a CH_3OH component give a better quantitative agreement. Within the error of over simplification in estimating the expected column densities of CO_2, we found that the values for our three sources with the best signal-to-noise ratio is compatible with the H_2O, CO (apolar), and CH_3OH components as obtained from the fit; instead, for our three-component fit we find a worse agreement with the expected abundance of the polar component.

The above-mentioned result could be an indirect correlation between the degradation of CH_3OH and the formation of CO_2. Both molecules are believed to be formed in the solid-state primarily from accreted CO on the grain surface. However, observations have revealed CO_2 to be an abundant constituent of ices in the dark molecular clouds, whereas CH_3OH abundance extends from upper limits to weak detections in several lines of sight. The column densities are listed in Table 4 for comparison. Moreover, laboratory experiments indicate that CO_2 can efficiently be formed by energetic processing of CH_3OH (e.g. Baratta et al. 2002; Modica & Palumbo 2010; Islam et al. 2014). Hence, CH_3OH is most likely formed in the early stages of dark clouds through the hydrogenation of CO ice (Watanabe et al. 2004; Fuchs et al. 2009), and it is partially used up to form CO_2.

In addition, we would like to point out that in the mixtures considered in this study, CO_2 is not the only species formed after ion irradiation (see Fig. 2). The features due to the other species formed should also be present in the spectra observed along the same lines of sight if cosmic ion irradiation is active in the quiescent regions. In the case of pure CO, carbon dioxide is the most abundant species formed (about 10% with respect to initial CO), while carbon chain oxides (such as C_2O, C_3O, and C_3O_2) are formed with an abundance of the order of 0.1% with respect to the initial CO (e.g. Gerakines & Moore 2001; Trottier & Brooks 2004; Loeffler et al. 2005; Palumbo et al. 2008). In the case of CO:N_2 mixtures, again carbon dioxide is the most abundant species formed while carbon chain oxides and nitrogen oxides (such as NO, N_2O, and NO_2) are formed with an abundance of the order of 0.1% (Ioppolo et al. 2009; Sicilia et al. 2012). The IR features due to solid carbon chain oxides and nitrogen oxides would be too weak to be detected in the line of sight to dense molecular clouds with current astronomical instrumentation; however, C_2O, C_3O, NO, and N_2O have been detected in the gas phase, with an abundance with respect to hydrogen of the order of 10^{-10}–10^{-8} because of their rotational transitions at radio wavelengths (e.g. Matthews et al. 1984; Brown et al. 1985; Ohishi et al. 1991; Ziurys et al. 1994; Halfen et al. 2001; Palumbo et al. 2008). Based on the comparison between the laboratory data and astronomical observations it has been suggested that in dense molecular clouds gas phase carbon chain oxides and nitrogen oxides are formed in the solid phase after cosmic ion irradiation of icy grain mantles and are released to the gas phase after the desorption of grain mantles (Palumbo et al. 2008; Sicilia et al. 2012).

When a sample of H_2O deposited on C-grains is considered, both CO and CO_2 are formed after ion irradiation with a comparable column density. As discussed by Mennella et al. (2004), the spectral profile and the contribution to the observed column densities make solid CO formed by cosmic-ray irradiation of ice-layered carbon grains a good candidate for the red component (at about 2136 cm^{-1}) of the interstellar CO stretching feature, which is generally attributed to CO mixed with water ice or to CO mixed with CH_3OH (e.g. Palumbo & Strazzulla 1992; Cuppen et al. 2011). According to Pontoppidan et al. (2003), the red component accounts for about 10% to 60% of total CO column density. Mennella et al. (2004) have found that the column density of CO formed after cosmic-ion irradiation of ice-layered C-grains can give a contribution of 3–36% to the total observed column density suggesting that an additional feature could contribute to the red component.

After ion irradiation of solid methanol, several absorption features are present in the IR spectra which are assigned to molecular species formed after irradiation. The most abundant are CO, CO_2, formaldehyde (H_2CO), and methane (CH_4) (e.g. Hudson & Moore 2000; Baratta et al. 2002). As shown by Palumbo & Strazzulla (1993), Chiar et al. (1995), and Teixeira et al. (1998), the profile of the CO band produced after ion irradiation of methanol reproduces well the red component of the interstellar CO stretching feature. The most intense IR band of H_2CO in the solid phase occurs at about 1720 cm^{-1} (5.8 μm). In astronomical spectra, this feature is expected to be blended in with the broad 1660 cm^{-1} (6.0 μm) water band and in fact it has been suggested that formaldehyde could contribute to the C1 component of the interstellar 5–8 μm absorption feature (Boogert et al. 2008) in the line of sight to young stellar objects. In laboratory spectra of irradiated methanol samples, the abundance of H_2CO is of the order of 10% with respect to methanol which would make the contribution of formaldehyde to the 6 μm band observed in the line of sight to background sources almost negligible, in agreement with the analysis of the 5–8 μm absorption feature observed towards field stars presented by Knez et al. (2005). The column density of CH_4 formed after ion irradiation of methanol is expected to be of the order of 10% with respect to observed methanol (Baratta et al. 2002) and the intensity of its absorption bands would be below the detection limit of current astronomical instrumentation in the line of sight to background sources. Other species such as methyl formate, ethylene glycol, and glycolaldehyde are formed after ion irradiation of methanol-rich samples with an abundance of the order of 0.1% with respect to methanol (e.g. Hudson & Moore 2000; Modica & Palumbo 2010). The absorption features of these species would be too weak to be detected in interstellar ices; however, it is generally

accepted that the amount formed in the solid phase contributes to the gas phase abundance after desorption of icy grain mantles (e.g. Öberg et al. 2009; Modica & Palumbo 2010; Chuang et al. 2017).

5. Conclusion

Laboratory spectra of ion irradiated mixtures are used to fit the profile of the solid CO_2 bending mode band observed by the *Spitzer* Space Telescope in the line of sight to quiescent dark cloud regions (i.e. background sources). From a qualitative point of view, good fits are obtained by using either three or four components. From a quantitative point of view, a better result is obtained with four components, i.e. when the spectrum of CO_2 formed after ion irradiation of CH_3OH is added to the fitting procedure. The results presented support the hypothesis that energetic processing of icy grain mantles can be an efficient means by which CO_2 is formed in quiescent dark cloud regions; furthermore, this finding indirectly suggests the presence of CH_3OH in icy grain mantles in these cold regions. Owing to the intrinsic weakness of background stars, only a few spectra with a good signal-to-noise ratio have been obtained by the *Spitzer* Space Telescope. We expect that the *James Webb* Space Telescope (JWST) will be able to study the profile of the CO_2 bands towards a larger sample of background sources. In the near future, the comparison between new observations and laboratory spectra will provide us with a better knowledge of the chemical composition and physical properties of icy grain mantles in quiescent dense molecular clouds.

Acknowledgements. The authors are grateful to D. C. B. Whittet for the IRS *Spitzer* Space Telescope data and to V. Greco for writing an updated version of the Polyfit software. This research has been partially supported by the European COST Action CM 1401, Our Astro-Chemical History: Short Term Scientific Missions (STSM), the Italian Ministero dell'Istruzione, dell'Università e della Ricerca through the grant Progetti Premiali 2012-iALMA (CUP C52I13000140001), the NRW International Graduate School of Chemistry, Münster, and the LASSIE Initial Training Network, which is supported by the European Community's Seventh Framework Programme under Grant Agreement Number 238258. S.I. acknowledges the Royal Society for financial support.

References

Allamandola, L. J., Sandford, S. A., & Valero, G. J. 1988, Icarus, 76, 225
Baratta, G. A., & Palumbo, M. E. 1998, J. Opt. Soc. Am. A, 15, 3076
Baratta, G. A., Palumbo, M. E., & Strazzulla, G. 2000, A&A, 357, 1045
Baratta, G. A., Leto, G., & Palumbo, M. E. 2002, A&A, 384, 343
Bergin, E. A., Melnick, G. J., Gerakines, P. A., Neufeld, D. A., & Whittet, D. C. B. 2005, ApJ, 627, L33
Bernstein, M. P., Sandford, S. A., Allamandola, L. J., Chang, S., & Scharberg, M. A. 1995, ApJ, 454, 327
Boogert, A. C. A., Pontoppidan, K. M., Knez, C., et al. 2008, ApJ, 678, 1004
Boogert, A. C. A., Huard, T. L., Cook, A. M., et al. 2011, ApJ, 729, 92
Boogert, A. C. A., Gerakines, P. A., & Whittet, D. C. B. 2015, ARA&A, 53, 541
Boonman, A. M. S., van Dishoeck, E. F., Lahuis, F., Wright, C. M., & Doty, S. D. 2003, A&A, 399, 1063
Brown, R. D., Godfrey, P. D., Cragg, D. M., et al. 1985, ApJ, 297, 302
Chiar, J. E., Adamson, A. J., Kerr, T. H., & Whittet, D. C. B. 1994, ApJ, 426, 240
Chiar, J. E., Adamson, A. J., Kerr, T. H., & Whittet, D. C. B. 1995, ApJ, 455, 234
Chiar, J. E., Pendleton, Y. J., Allamandola, L. J., et al. 2011, ApJ, 731, 9
Chuang, K.-J., Fedoseev, G., Qasim, D., et al. 2017, MNRAS, 467, 2552
Cuppen, H. M., Penteado, E. M., Isokoski, K., van der Marel, N., & Linnartz, H. 2011, MNRAS, 417, 2809
Dartois, E., Demyk, K., d'Hendecourt, L. B., & Ehrenfreund, P. 1999, A&A, 351, 1066
d'Hendecourt, L. B., Allamandola, L. J., Grim, R. J. A., & Greenberg, J. M. 1986, A&A, 158, 119
d'Hendecourt, L. B., & Jourdain de Muizon, M. 1989, A&A, 223, L5
de Graauw, T., Whittet, D. C. B., Gerakines, P. A., et al. 1996, A&A, 315, L345
Ehrenfreund, P., Boogert, A. C. A., Gerakines, P. A., et al. 1996, A&A, 315, L341
Ehrenfreund, P., Boogert, A. C. A., Gerakines, P. A., Tielens, A. G. G. M., & van Dishoeck, E. F. 1997, A&A, 328, 649
Eiroa, C., & Hodapp, K. W. 1989, A&A, 210, 345
Fuchs, G. W., Cuppen, H. M., Ioppolo, S., et al. 2009, A&A, 505, 629
Garozzo, M., La Rosa, L., Kanuchova, Z., et al. 2011, A&A, 528, A118
Gerakines, P. A., & Moore, M. H. 2001, Icarus, 154, 372
Gerakines, P. A., Schutte, W. A., Greenberg, J. M., & van Dishoeck, E. F. 1995, A&A, 296, 810
Gerakines, P. A., Schutte, W. A., & Ehrenfreund, P. 1996, A&A, 312, 289
Gerakines, P. A., Whittet, D. C. B., Ehrenfreund, P., et al. 1999, ApJ, 522, 357
Gibb, E. L., Whittet, D. C. B., Boogert, A. C. A., & Tielens, A. G. G. M. 2004, ApJS, 151, 35
Goumans, T. P. M., Uppal, M. A., & Brown, W. A. 2008, MNRAS, 384, 1158
Halfen, D. T., Apponi, A. J., & Ziurys, L. M. 2001, ApJ, 561, 244
Hudgins, D. M., Sandford, S. A., Allamandola, L. J., & Tielens, A. G. G. M. 1993, ApJS, 86, 713
Hudson, R. L., & Moore, M. H. 1999, Icarus, 140, 451
Hudson, R. L., & Moore, M. H. 2000, Icarus, 145, 661
Ioppolo, S., Palumbo, M. E., Baratta, G. A., & Mennella, V. 2009, A&A, 493, 1017
Ioppolo, S., van Boheemen, Y., Cuppen, H. M., van Dishoeck, E. F., & Linnartz, H. 2011, MNRAS, 413, 2281
Ioppolo, S., Fedoseev, G., Lamberts, T., Romanzin, C., & Linnartz, H. 2013a, Rev. Sci. Instr., 84, 073112-073112-13
Ioppolo, S., Sangiorgio, I., Baratta, G. A., & Palumbo, M. E. 2013b, A&A, 554, A34
Islam, F., Baratta, G. A., & Palumbo, M. E. 2014, A&A, 561, A73
Jamieson, C. S., Mebel, A. M., & Kaiser, R. I. 2006, ApJS, 163, 184
Jenniskens, P., Baratta, G. A., Kouchi, A., et al. 1993, A&A, 273, 583
Jiang, G. J., Person, W. B., & Brown, K. G. 1975, J. Chem. Phys., 62, 1201
Kaňuchová, Z., Urso, R. G., Baratta, G. A., et al. 2016, A&A, 585, A155
Keane, J. K., Boogert, A. C. A., Tielens, A. G. G. M., Ehrenfreund, P., & Schutte, W. A. 2001, A&A, 375, L43
Knez, C., Boogert, A. C. A., Pontoppidan, K. M., et al. 2005, ApJ, 635, L145
Lacy, J. H., Faraji, H., Sandford, S. A., & Allamandola, L. J. 1998, ApJ, 501, L105
Laffon, C., Lasne, J., Bournel, F., et al. 2010, Phys. Chem. Chem. Phys., 12, 10865
Liu, T., Wu, Y., & Zhang, H. 2013, ApJ, 775, L2
Loeffler, M. J., Baratta, G. A., Palumbo, M. E., Strazzulla, G., & Baragiola, R. A. 2005, A&A, 435, 587
Matthews, H. E., Irvine, W. M., Friberg, P., Brown, R. D., & Godfrey, P. D. 1984, Nature, 310, 125
Mennella, V., Baratta, G. A., Esposito, A., Ferini, G., & Pendleton, Y. J. 2003, ApJ, 587, 727
Mennella, V., Palumbo, M. E., & Baratta, G. A. 2004, ApJ, 615, 1073
Mennella, V., Baratta, G. A., Palumbo, M. E., & Bergin, E. A. 2006, ApJ, 643, 923
Minissale, M., Congiu, E., Manicó, G., Pirronello, V., & Dulieu, F. 2013, A&A, 559, A49
Minissale, M., Loison, J.-C., Baouche, S., et al. 2015, A&A, 577, A2
Modica, P., & Palumbo, M. E. 2010, A&A, 519, A22
Moore, M. H., Khanna, R., & Donn, B. 1991, J. Geophys. Res., 96, 17541
Mulas, G., Baratta, G. A., Palumbo, M. E., & Strazzulla, G. 1998, A&A, 333, 1025
Murakawa, K., Tamura, M., & Nagata, T. 2000, ApJS, 128, 603
Noble, J. A., Dulieu, F., Congiu, E., & Fraser, H. J. 2011, ApJ, 735, 121
Nummelin, A., Whittet, D. C. B., Gibb, E. L., Gerakines, P. A., & Chiar, J. E. 2001, ApJ, 558, 185
Oba, Y., Watanabe, N., Kouchi, A., Hama, T., & Pirronello, V. 2010, ApJ, 722, 1598
Öberg, K. I., Garrod, R. T., van Dishoeck, E. F., & Linnartz, H. 2009, A&A, 504, 891
Öberg, K., Boogert, A. C. A., Pontoppidan, K. M., et al. 2011, ApJ, 740, 109
Ohishi, M., Suzuki, H., Ishikawa, S., et al. 1991, ApJ, 380, L39
Palumbo, M. E., & Strazzulla, G. 1992, A&A, 259, L12
Palumbo, M. E., & Strazzulla, G. 1993, A&A, 269, 568
Palumbo, M. E., Baratta, G. A., Brucato, J. R., et al. 1998, A&A, 334, 247
Palumbo, M. E., Castorina, A. C., & Strazzulla, G. 1999, A&A, 342, 551
Palumbo, M. E., Baratta, G. A., Collings, M. P., & McCoustra, M. R. S. 2006, Phys. Chem. Chem. Phys., 8, 279
Palumbo, M. E., Leto, P., Siringo, C., & Trigilio, C. 2008, ApJ, 685, 1033
Pontoppidan, K. M., Fraser, H. J., Dartois, E., et al. 2003, A&A, 408, 981

Pontoppidan, K. M., Dullemond, C. P., van Dishoeck, E. F., et al. 2005, ApJ, 622, 463
Pontoppidan, K. M., Boogert, A. C. A., Fraser, H. J., et al. 2008, ApJ, 678, 1005
Prasad, S. S., & Tarafdar, S. P. 1983, ApJ, 267, 603
Raut, U., & Baragiola, R. 2011, ApJ, 737, L14
Raut, U., Fulvio, D., Loeffler, M. J., & Baragiola, R. A. 2012, ApJ, 752, 159
Roser, J. E., Vidali, G., Manicó, G., & Pirronello, V. 2001, ApJ, 555, L61
Rothard, H., Domaracka, A., Boduch, P., et al. 2017, J. Phys. B, 50, 062001
Shen, C. J., Greenberg, J. M., Schutte, W. A., & van Dishoek, E. F. 2004, A&A, 415, 203
Sicilia, D., Ioppolo, S., Vindigni, T., Baratta, G. A., & Palumbo, M. E. 2012, A&A, 543, A155
Smith, R. G., Sellgren, K., & Brooke, T. Y. 1993, MNRAS, 263, 749
Strazzulla, G., & Johnson, R. E. 1991, Astrophys. Space Sci. Lib., 167, 243
Talbi, D., Chandler, G. S., & Rohl, A. L. 2006, Chem. Phys., 320, 214
Teixeira, T. C., Emerson, J. P., & Palumbo, M. E. 1998, A&A, 330, 711
Tielens, A. G. G. M., & Hagen, W. 1982, A&A, 114, 245
Trottier, A., & Brooks, R. L. 2004, ApJ, 612, 1214
Urso, R. G., Sciré, C., Baratta, G. A., Compagnini, G., & Palumbo, M. E. 2016, A&A, 594, A80
Valentijn, E. A., & Thi, W. F. 2000, Exp. Astron., 10, 215
van Dishoeck, E. F., Helmich, F. P., de Graauw, T., et al. 1996, A&A, 315, L349
van Dishoeck, E. F., Herbst, E., & Neufeld, D. A. 2013, Chem. Rev., 113, 9043
Watanabe, N., & Kouchi, A. 2002, ApJ, 567, 651
Watanabe, N., Nagaoka, A., Shiraki, T., & Kouchi, A. 2004, ApJ, 616, 638
Watanabe, N., Mouri, O., Nagaoka, T., et al. 2007, ApJ, 668, 1001
Werner, M. W., Roellig, T. L., Low, F. J., et al. 2004, ApJS, 154, 1
Whittet, D. C. B., Bode, M. F., Longmore, A. J., et al. 1988, MNRAS, 233, 321
Whittet, D. C. B., Gerakines, P. A., Tielens, A. G. G. M., et al. 1998, ApJ, 498, L159
Whittet, D. C. B., Shenoy, S. S., Bergin, E. A., et al. 2007, ApJ, 655, 332
Whittet, D. C. B., Cook, A. M., Chiar, J. E., et al. 2009, ApJ, 695, 94
Yamada, H., & Person, W. B. 1964, J. Chem. Phys., 41, 2478
Ziegler, J. F., Ziegler, M. D., & Biersack, J. P. 2008, The stopping and range of ions in solids (New York: Pergamon Press), http://www.srim.org
Ziurys, L. M., Apponi, A. J., Hollis, J. M., & Snyder, L. E. 1994, ApJ, 436, L181